Journal of Sciences, Islamic Republic of Iran 35(1): 41 - 54 (2024) http://jsciences.ut.ac.ir
University of Tehran, ISSN 1016-1104

Tectonic Setting of the Serow-Torshab Ophiolite Related Mafic Rocks, NW-Iran: Implications from Minerals and Whole-Rock Geochemistry

M. Modjarrad[1*], I. Uysal[2]

[1] *Department of Geology, faculty of science, Urmia University, Urmia, Islamic Republic of Iran*
[2] *Department of Geological Engineering, Karadeniz Technical University, 61080 Trabzon, Türkiye*

Received: 13 July 2024 / Revised: 28 August 2024 / Accepted: 30 September 2024

Abstract

In this paper, focused on the Late Cretaceous Serow ophiolite related gabbros from the Torshab area, NW Iran, to enhance our understanding on the tectonic setting of ophiolite formation in terms of pressure-temperature and fluid conditions. The applied methods encompassed field geological observations, petrographic and mineralogical analyses, and whole-rock chemistry assessments. The findings revealed that the calc-alkaline gabbros predominantly consist of hornblende gabbro, olivine gabbro, and minerals such as amphibole, ortho-/clinopyroxene, olivine, and plagioclase. According to geochemical signatures such as the depletion of high field strength elements (Hf, Zr, Nb, and Ta) and the enrichment of large ionic lithophile elements (Ba and K) the Serow-Torshab gabbro is considered in relation to an arc setting indicating their origin from a mantle wedge, potentially enriched by subducting crust-derived melts/fluids. The mineral chemical study on mafic phases also suggests a supra-subduction zone (SSZ, fore-arc) environment for the Serow ophiolite, offering valuable insights into the region's geodynamic evolution.

Keywords: Ophiolite-Related Gabbro; Fore-Arc Setting; Mineral Chemistry; Serow-Torshab; NW Iran Ophiolites.

Introduction

The ophiolitic fragments cropped out in Neo-Tethyan suture zones spanning from NW Iran through Iraqi Zagros to the Baer-Basit (border of Türkiye - Syria) exhibit numerous correspondences in their tectonic settings of generation (supra-subduction zone or mid-ocean ridge), age (predominantly Late Cretaceous, around 100-90 million years), and lithologies (1, 2 and references therein). Most of the Late Cretaceous Neo-Tethyan ophiolites, especially in NW Iran, are believed to have formed in an SSZ environment (3) or an abyssal setting (4). These ophiolites were formed during the collision between the Arabi-Eurasian (Central-Iranian) plates in various locations such as Kermanshah (Harsin), Kamyaran (Garmab), Marivan (Sarvabad), Piranshahr, Sardasht, Silvana (Gysian), and Serow near Urmia (1). In many instances, mafic bodies, particularly gabbros, are found alongside ultramafic rocks or within ophiolitic melanges. Investigating these gabbros aids in enhancing our comprehension of the ophiolites. The chemical characteristics of mafic minerals in these gabbros, particularly amphibole and pyroxene, can offer valuable insights into interpreting the physicochemical nature and conditions of the source magma (5). The hornblende-bearing gabbros are a common rock type in subduction-related magmatic assemblages and indicate fractional magmatic processes in an arc setting (6, 7). The

[*] Corresponding Author: Tel: 04433441932; Email: m.modjarrad@urmia.ac.ir

hornblende in subduction-related ophiolitic gabbros may form as the primary phase from hydrous mafic magma (8) or as a reaction product of primary mafic minerals (9).

Additionally, due to the constant companionship between ophiolites and gabbros (layered or massive types), the study of the Serow ophiolite-related gabbros concerning their mineral and whole rock chemistry accompanied with petrogenetic and tectonic setting indications, could help to evaluation the Neo-Tethyan characteristics in this part of the suture, at NW Iran.

Our study has specifically focused on the Serow-Torshab ophiolite-related gabbros found in the Torshab area as a small stock in NW Iran (Figure 1). Field geological observations, petrographic analyses, and mineralogical and whole-rock chemistry data were utilized to delve into the pressure-temperature (PT) conditions and petrogenesis of these gabbros. While whole-rock chemistry and crystal size distribution have already been studied in these gabbros (10), to the best of our knowledge, mineral chemistry data have not been investigated yet.

Geological setting

The study area is situated in the northwest of Urmia (Figure 2) on the Serow 1:250.000 sheet scaled geological map of the Geological Society of Iran (12) and the 1:100.000 scaled Gangechin map (13). The mafic stocks in the vicinity of Urmia are part of the Urmia-Dokhtar magmatic arc (14), associated with the subduction and closure of the Neo-Tethyan ocean. Within the study area, small gabbroic patches have intruded metamorphic and sedimentary rocks dating back to the Early Paleozoic era (12, Figure 3).

A notable characteristic surrounding the medium to coarse-grained gabbroic rocks is the presence of high-Ti placer deposits in the Serow area. These deposits contain significant quantities of Ti-rich minerals such as ilmenite, diopside, and amphiboles, which were abundant phases found within the historical drainage pattern of the area.

The igneous rocks (both mafic and acidic) in the Serow region intruded during the Late Mesozoic to Early Cenozoic periods due to the collision between the Iranian and Arabian plates (15). The Serow ophiolitic fragment, situated in northwest Iran near the Iran-Türkiye border, shares similarities with other Neo-Tethyan Mesozoic ophiolites in northwest Iran (e.g., Gysian), manifesting as a tectonic mélange which is predominantly composed of serpentinized ultramafic rocks (lherzolitic-harzburgites and some dunites), basaltic lavas, diabases, Upper Cretaceous limestones (pelagic and radiolarite/globotruncana-bearing), as well as sedimentary rocks such as sandstone and shale.

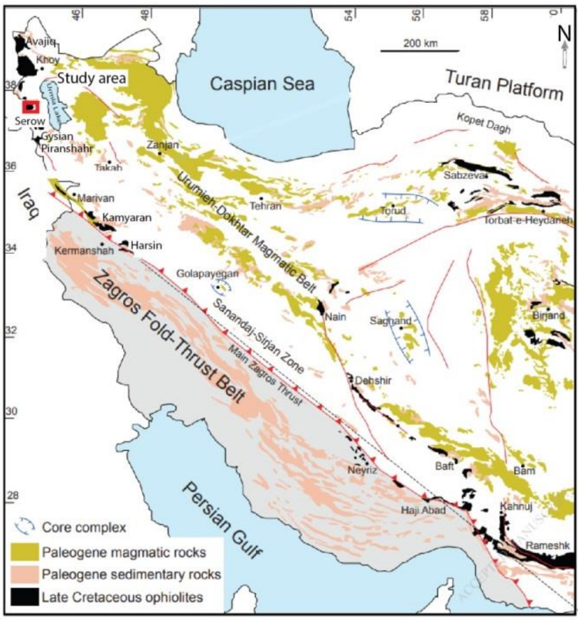

Figure 1. Geological map of Iran depicting Paleogene magmatic and sedimentary rocks as well as Late Cretaceous ophiolites (modified after 11). The study area, Serow (highlighted in a red box), along with other ophiolitic fragments in West Azarbaijan Province including Avajiq, Khoy, Serow, Gysian, and Piranshahr are situated in this region. Notable well-recognized fragments like Marivan, Kamyaran (Garmab), and Harsin in the Zagros Ophiolite Belt (ZOB) are also indicated.

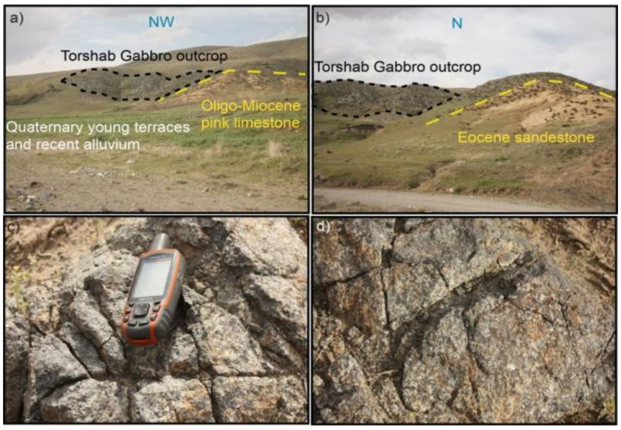

Figure 2. a, b) Field photos of the Serow, Torshab region and related units.c, d) The mesoscopic scale of the Torshab coarse-grained gabbro.

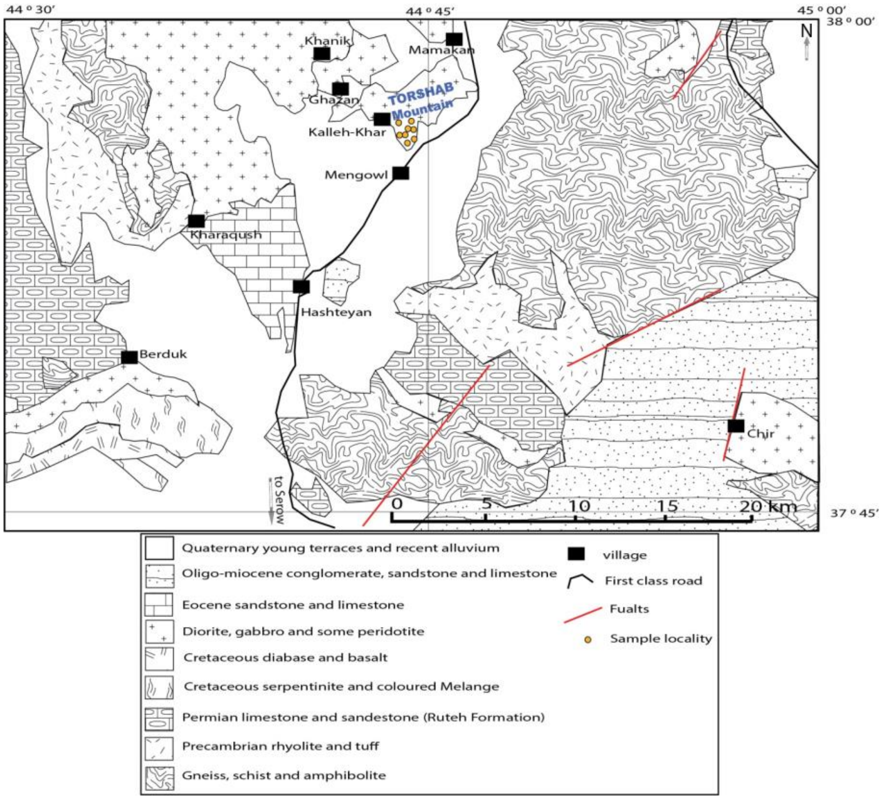

Figure 3. The simplified geological map of Serow-Torshab area (modified after 12; 1:250.000 scaled map), showing the location of the analyzed samples indicated by blue, yellow and black stars.

Triassic and Jurassic sedimentary rocks are not exposed in the area; instead, Cretaceous units are prevalent. Contact metamorphic aureoles have developed around the basic intrusions and near the Permian limestones, leading to the formation of some garnet, wollastonite, and diopside-bearing skarn deposits, notably encompassing the Ghazan patch. Gabbroic rocks within the Serow-Torshab area intruded the ultramafic unit in the form of several intrusive stocks in the Serow area (Figure 3), including Ghazan (16), Khanik (17), Chir, Moskin (10), and Torshab (from this study). The studied rocks, appearing as stocks (small patches), exhibit dark green-brownish-black colors, with the feldspar-bearing portions appearing lighter.

Materials and Methods

Numerous mafic rocks were sampled from the Serow-Torshab Mountain, located near the Iran-Türkiye border, following thorough fieldwork conducted during the summers of 2019 and 2020. After initial petrographic assessments, a careful selection of samples was made for electron microprobe analysis (EPMA). Subsequently, three mafic thin sections underwent detailed examination. The EPMA were carried out at the Department of Earth and Environmental Sciences at Ludwig Maximilian University in Munich, Germany, by utilizing a Cameca SX-100 system equipped with a LaB6 cathode. This fully automated instrument incorporates five wavelength dispersive spectrometers for nondestructive analysis. Various phases, such as olivine, pyroxenes, plagioclase, and amphibole, among others, were analyzed and reference materials were employed to calibrate the EPMAs. The data obtained from the EPMA are outlined in Table 1.

After conducting petrographic and EPMA studies on mineral assemblages and textures, eight representative samples from the Serow-Torshab (near the Chir village) were selected for geochemical analysis (Table 2). Whole-rock major- and trace-element ICP-OES analysis utilizing a radial 735 model and V-Groove nebulizer with a detection limit of 0.05% dl, was performed using a spectro-analytical instrument at the ZarAzma Laboratory in Tehran, Iran. The aqua-regia digestion method involving hydrochloric and nitric acids, which is suitable for various exploration applications and provides a cost-effective multi-element analysis solution for most base-metal explorers, was employed for the analyses (Table 2).

Results

Table 1. Representative mineral chemical compositions, along with cation distributions, for various phases analyzed from the Serow-Torshab gabbros, including olivine, orthopyroxene, clinopyroxene, plagioclase, amphibole, and serpentine. Mineral abbreviations follow the conventions outlined in reference 18 (Ol:olivine, opx: orthopyroxene, Cpx: clinopyroxene, Pl: plagioclase, Amp: amphibole, Srp: serpentine), with the analyzed point numbers denoted by "N."bdl: below detection limits.

	Ol	**Opx**	**Cpx**	**Pl**	**Amp**	**Srp**
Sample Name	*S10* N=11	*S9, S10* N=4	*S9, S10* N=15	*S9, S10* N=9	*S9, S10* N=45	*S9* N=8
SiO_2	37.03	54.42	53.06	43.30	43.29	35.03
TiO_2	bdl	0.15	0.29	0.03	0.08	0.03
Al_2O_3	bdl	1.52	1.93	32.86	12.60	0.24
Cr_2O_3	0.03	0.00	0.01	0.00	0.00	0.01
NiO	0.05	0.03	0.01	bdl	0.03	bdl
FeO	26.34	17.45	6.48	0.35	10.24	33.01
MgO	36.48	26.39	15.71	0.04	15.91	0.68
MnO	0.50	0.52	0.23	0.02	0.17	25.91
CaO	0.02	0.89	23.21	21.49	11.29	0.48
Na_2O	bdl	bdl	0.09	1.44	1.95	bdl
K_2O	bdl	0.02	bdl	0.03	0.28	0.01
P_2O_5	bdl	0.01	0.01	0.02	0.00	bdl
Cl	bdl	0.01	0.01	0.61	0.02	bdl
Total	100.45	101.41	101.07	100.23	95.97	95.44
	3C/4O	*4C/6O*	*4C/6O*	*5C/8O*	*15C/23O*	*5C/7O*
Si	0.977	1.949	1.935	2.040	6.270	1.706
Ti	-	0.004	0.008	0.001	0.012	-
Al	-	0.063	0.083	1.826	2.150	-
Cr	-	-	-	-	-	-
Fe^{3+}	0.029	0.031	-	0.014	0.901	0.015
Fe^{2+}	0.553	0.492	0.198	-	0.343	1.668
Mn	0.011	0.016	0.007	0.001	0.020	0.032
Mg	1.435	1.409	0.854	0.003	3.441	1.832
Ca	0.001	0.035	0.907	1.085	1.750	3.198
Na	-	-	0.007	0.133	0.553	-
K	-	-	-	0.002	0.051	-
Total	3.006	3.999	3.999	5.105	15.491	8.451
$Al^{(IV)}$	-	0.051	0.065	-	1.73	-
$Al^{(VI)}$	-	0.013	0.019	-	0.43	-
Mg #	72.2	74.1	81.2	-	90.9	52.3

Table 2. Whole-rock major oxides (wt. %) and trace element (ppm) contents as well as some ratios for the Serow-Torshab gabbros.

Sample	S1	S2	S3	S4	S5	S6	S7	S8
SiO_2	51.93	47.44	49.69	50.80	45.87	47.49	45.20	45.99
TiO_2	1.21	0.90	0.54	0.78	3.95	2.60	1.25	0.61
Al_2O_3	15.14	14.90	15.48	14.73	13.00	13.95	14.15	15.64
Fe_2O_3	10.00	10.72	9.46	8.95	15.98	13.87	13.43	9.18
MnO	0.15	0.19	0.17	0.16	0.20	0.28	0.20	0.16
MgO	6.45	9.18	7.45	8.52	5.64	6.77	8.19	12.02
CaO	8.27	11.03	10.89	11.15	9.79	9.56	10.91	12.17
Na_2O	3.41	2.68	3.34	2.72	3.73	3.49	3.16	1.83
K_2O	1.20	0.78	0.69	0.58	0.54	0.45	0.45	0.10
P_2O_5	0.31	0.11	0.15	0.18	0.19	0.30	0.26	0.12
LOI	1.74	1.86	1.92	1.32	0.9	1.06	2.43	1.92
Total	99.81	99.79	99.78	99.89	99.79	99.82	99.63	99.74
Ba	1491	187	456	324	243	305	172	51
Rb	23.37	16.54	12.19	14.63	10.04	8.28	9.67	3.13
Sr	252	171	329	190	421	336	222	120
Y	25.4	16.65	26.83	21.08	11.59	18.86	19.32	10.95
Zr	15.36	12.39	62.57	11.88	17.23	12.83	17.85	28.45
Nb	7.93	1.26	5.85	2.27	8.32	14.18	1.8	0.74
Th	1.02	<0.01	0.28	0.84	2.14	0.37	0.16	<0.01
Pb	1.49	3.02	<0.01	<0.01	0.24	<0.01	<0.01	<0.01
Ga	19.72	15.49	17.23	15.12	18.57	16.13	15.19	12.23
Cu	9.79	26.85	9.84	19.71	35.28	36.94	12.46	53.79
Ni	21	110	91	49	12	69	76	166
V	2.7	2.2	1.7	2.2	4	1.7	2.2	1.7
Hf	0.65	0.59	2.01	0.62	0.91	0.73	0.83	0.74
Cs	0.3	0.25	0.27	0.21	0.1	<0.01	0.2	0.12
Ta	0.32	<0.001	0.3	<0.01	0.56	1.26	<0.01	<0.01
Co	36.08	44.86	31.37	37.53	41.11	38.34	39.16	49.94
U	0.16	<0.01	<0.01	0.22	0.3	<0.01	<0.01	<0.01
W	1	0.67	1.33	0.4	0.91	1.8	2.64	0.88
Cr	89	303	231	426	49	183	160	529
La	24.13	1.4	8.28	5.86	8.74	5.63	3.45	1.31
Ce	61.71	4.07	18.31	12.76	16.16	12.97	8.09	3.1
Pr	7.95	1.02	3.52	2.42	2.64	2.57	1.7	0.72
Nd	35.46	7.32	21.93	15.08	15.09	16.36	11.12	4.75
Sm	7.58	2.04	4.82	3.31	2.77	3.55	2.64	1.24
Eu	2.34	0.76	1.98	1.03	1.25	1.81	1.24	0.51
Gd	6.56	2.41	4.93	3.52	2.8	3.82	3.12	1.56
Tb	1.16	0.57	1.06	0.78	0.53	0.78	0.7	0.36
Dy	6.08	3.62	6.32	4.68	2.72	4.3	4.04	2.2
Ho	1.29	0.83	1.35	1.05	0.56	0.93	0.91	0.5
Er	3.13	2.1	3.29	2.63	1.32	2.31	2.34	1.29
Tm	0.68	0.47	0.71	0.59	0.26	0.49	0.51	0.29
Yb	3.39	2.38	3.44	2.92	1.26	2.43	2.57	1.46
Lu	0.39	0.24	0.34	0.29	0.13	0.25	0.25	0.14
Nb/Yb	2.34	0.53	1.7	0.78	6.6	5.84	0.7	0.5
Th/Yb	0.3	0.004	0.081	0.29	1.7	0.15	0.06	0.007
Zr/Y	0.6	0.74	2.33	0.56	1.49	0.68	0.92	2.6
Nb/Y	0.31	0.076	0.22	0.1	0.72	0.75	0.09	0.07
Sm/La	0.31	1.46	0.58	0.56	0.32	0.63	0.77	0.95
Th/La	0.04		0.03	0.14	0.24	0.07	0.05	
Zr/Nb	1.94	9.83	10.7	5.23	2.07	0.9	9.9	38.4

Petrographic descriptions and mineral composition

The intrusive rocks in the Serow-Torshab region primarily consist of gabbros, categorized into hornblende gabbro and olivine gabbro based on the modal percentage of the main phases and microstructures. The grain sizes are predominantly medium to coarse, displaying sub-/anhedral granular, intergranular, and poikilitic (sub-ophitic) textures (Figure 4).

The prevalent minerals in the Serow-Torshab gabbros are amphibole, clino-/ortho-pyroxene, olivine, and plagioclase, with occasional occurrences of serpentine. Polysynthetic twinning is common in relatively fresh, plagioclases, while pyroxenes primarily consist of clinopyroxene as individual crystals (heterogeneous

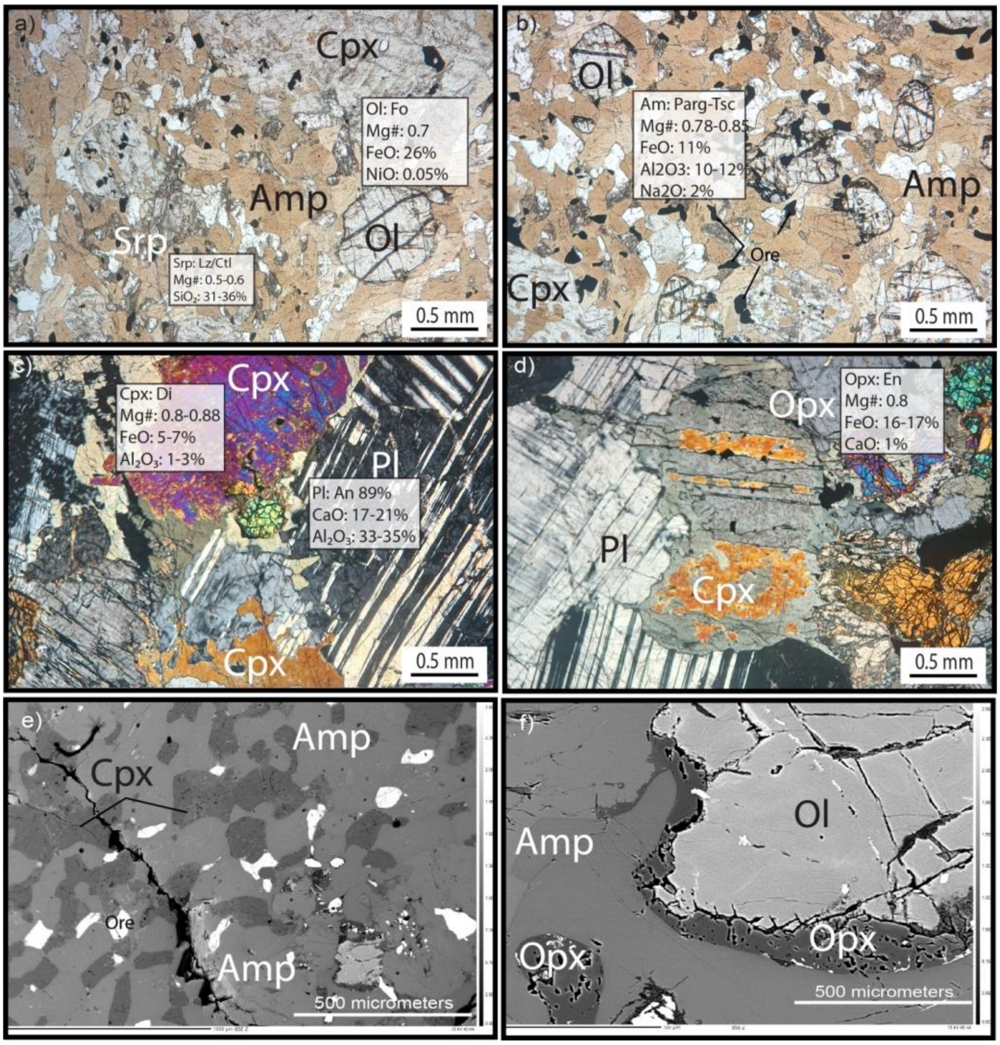

Figure 4. Microphotographs (a, b; plain-polarized and c, d; cross-polarized) and BSE images (e, f) of the Serow-Torshab gabbros. Summary of the mineral compositional data are shown on thin section photos (a-d). Mineral abbreviations are after 18. The EPMA data are presented in Table 1.

crystallization) or as exsolution lamellas within orthopyroxenes. Alteration to serpentine group minerals can be observed in the cracks of olivine. BSE images reveal narrow orthopyroxene rims forming around the olivines. In some samples, amphibole coarse grains encase clinopyroxenes intermittently. Following detailed petrographic studies, three representative thin sections underwent EPMAs.

Olivine crystals are predominantly forsterite-rich (chrysotile; Fo: 74, <10 modal%, Figure 5a), and altered to serpentine (Mg#: 0.52-0.60, <10 modal%), in most cases. Orthopyroxenes are primarily enstatite (Mg#: 0.76-0.79, Al_2O_3: 1.2 wt.%, <10 modal%), in direct association with diopsidic clinopyroxene crystals (Mg#: 0.85-0.89, Al_2O_3: up to 2 wt.%, 10-15 modal%). Anorthite contents in the plagioclases (An: 88-94, 15 modal%, Figure 5b) are high. Predominantly, hornblende gabbros encompass pargasite to magnesiohornblende-tschermakite amphiboles (Figure 6a; Mg#: 0.91, Al^{IV}: 1.7, Al^{VI}: 0.43, Na: 0.55 apfu, 40 modal%) within the rock matrix. Additionally, secondary tremolites, identified as the alteration products of pyroxenes, are present in some samples (Figure 6b).

Whole rock chemistry

The gabbros found in the Serow-Torshab area originate from basaltic magma (Figure 7a, diagram from 21) and typically exhibit SiO_2 contents ranging from 45-52 wt.% and MgO contents of 6.5-12 wt.% (Table 2). These gabbros display relatively high TiO_2 contents,

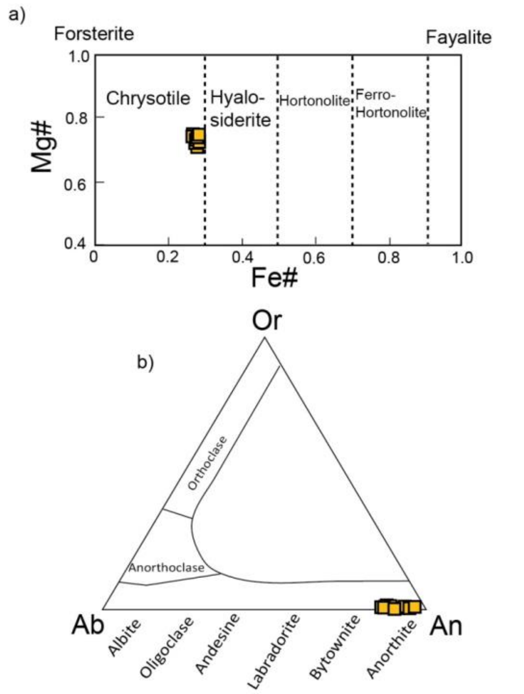

Figure 5. Mineral classification diagrams for olivine a) and feldspar. b) The olivines in Serow-Torshab gabbros are Mg-rich chrysotile, and their plagioclases are anorthite-rich (19).

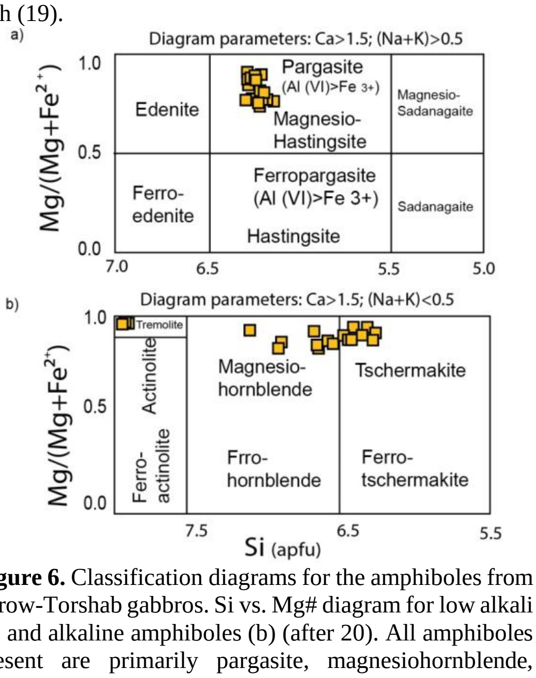

Figure 6. Classification diagrams for the amphiboles from Serow-Torshab gabbros. Si vs. Mg# diagram for low alkali (a) and alkaline amphiboles (b) (after 20). All amphiboles present are primarily pargasite, magnesiohornblende, transitioning to tschermakite, with occasional occurrences of secondary tremolite.

approximately in the range of 0.5-4 wt.%. Additionally, their CaO content falls between 8 wt.% and 12 wt.%. Al_2O_3 ranges from 13 wt.% and 15.5 wt.%, and $FeO_{(T)}$ is around 9-16 wt.%. The levels of Al_2O_3 and CaO are linked to the substantial modal proportions of plagioclase and clinopyroxene in these rocks. Furthermore, their Co content falls within the range of approximately 30-50 ppm, and Zr is between 12 ppm and 62 ppm. In addition Ni ranges from 20ppm and 160 ppm, and Y contents are between 11 ppm and 26 ppm. The high field strength elements (HFSE) like Hf, Ta, Th, and U contents are relatively low, ranging below 1-2 ppm.

Moreover, all Serow-Torshab gabbros exhibit a calc-alkaline to tholeiitic character (Figure 7b) mostly with an SSZ related affinity, as determined by trace element ratios such as Nb/Yb vs. Th/Yb and $Nb_{(N)}$ vs. $Th_{(N)}$ (Figure 7b, c). An arc setting is confirmed by other discrimination diagrams such as $FeO_{(T)}$-Alk-MgO ternary (Figure 7d), and Ti/40-Si/1000-Sr (Figure 7e) diagrams.

The chondrite-normalized Rare Earth Elements (REE) diagram (Figure 8a) of the Serow-Torshab gabbros exhibits a slight light REE/heavy REE (HREE) enrichment. In the N-MORB normalized multi-element diagram of the analyzed rocks (Figure 8b), there is notable enrichment in Large Ion Lithophile Elements (LILE), such as Ba, K, Sr, and Pb contents in contrast to depletion in HFSE.

Discussion

Tectonic setting

All the discrimination diagrams show an arc related setting for the Serow gabbros (Figure 7). The LREE/HREE enrichments at the Serow-Torshab gabbros (Figure 8a) could potentially reflect the enrichment of the mantle source of gabbros with subducted oceanic crust-derived components. Consequently, the gabbro could represent a segment of the lithospheric mantle enriched in incompatible elements (e.g., LREE; Figure 8b). The island arc basalt (IAB)-like pattern in the multi-element diagram of the Serow-Torshab gabbros, especially enrichment in LILE may indicate the generation at an arc tectonic setting of the source magma (e.g., 29). The depleted HFSE such as Zr, Hf, Ta and Nb may indicate arc setting formation for the studied rocks (30). While, the positive Eu anomaly (Figure 8a) indicates the high abundance of plagioclase in the rock, a convex up pattern (Middle REE enrichment) can be interpreted by the dominant phase of amphibole presence (31).

The composition of the pargasitic-tschermakitic amphibole in the Serow-Torshab gabbro demonstrates a

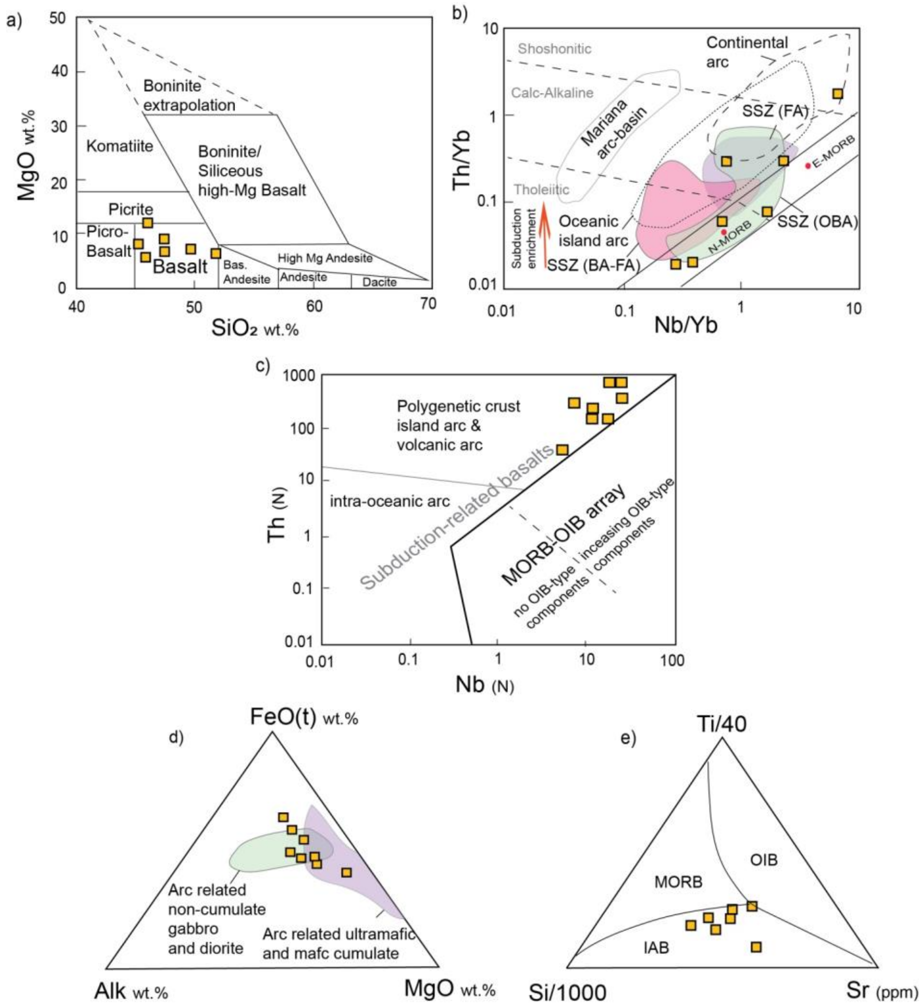

Figure 7. a) Distribution of MgO wt.% and SiO_2 wt.% contents of the Serow-Torshab gabbro on a high-Mg mafic to ultramafic-mafic rock discrimination diagram (21), all samples falling within the basalt field. b) The discrimination diagram of the Nb/Yb vs. Th/Yb (22), which shows a SSZ (OBA) affinity for the studied rocks. The SSZ setting fields are determined by colors and abbreviations are as following: SSZ (BA-FA): supra subduction zone back-arc to fore-arc, SSZ (OBA): supra subduction zone oceanic back-arc and SSZ (FA): supra subduction zone fore-arc setting. c) The Nb $_{(N)}$ vs. Th $_{(N)}$ diagram (23) which are normalized to the primitive mantle (PM values after 24). The diagram shows polygenetic crust island arc setting for the studied rocks. d) AFM discrimination ternary diagram for the Serow-Torshab gabbroic rocks. Fields of cumulate and non-cumulate rocks are from (25). e) The tectonic setting discrimination diagram (26), all the samples are located in the IAB field. The abbreviations are: OIB: oceanic island basalt, MORB: middle oceanic ridges basalt, IAB: island arc basalt. Complete whole rock data results are presented in Table 2.

magmatic origin (Figure 9a) and suggests formation within an SSZ setting (Figure 9b). Similar conclusions are drawn from the clinopyroxene composition (Figure 10a-c), indicating characteristics consistent with the SSZ environment. Moreover, clinopyroxenes from the Serow-Torshab gabbros point toward moderate pressure crystallization within the SSZ setting (Figure 10c). The clinopyroxenes in the Serow-Torshab gabbros also display an arc-related trend based on their Al and Ti contents (Figure 10d).

Mineral chemistry examinations of the serpentinized peridotites of the Serow ultramafics in the southwestern part of the Serow-Torshab gabbroic patch indicate an SSZ setting for the Serow ophiolite (38). Nonetheless, the absence of comprehensive data on the whole-rock chemistry, particularly the REEs of the peridotites, hinders making definitive conclusions about them.

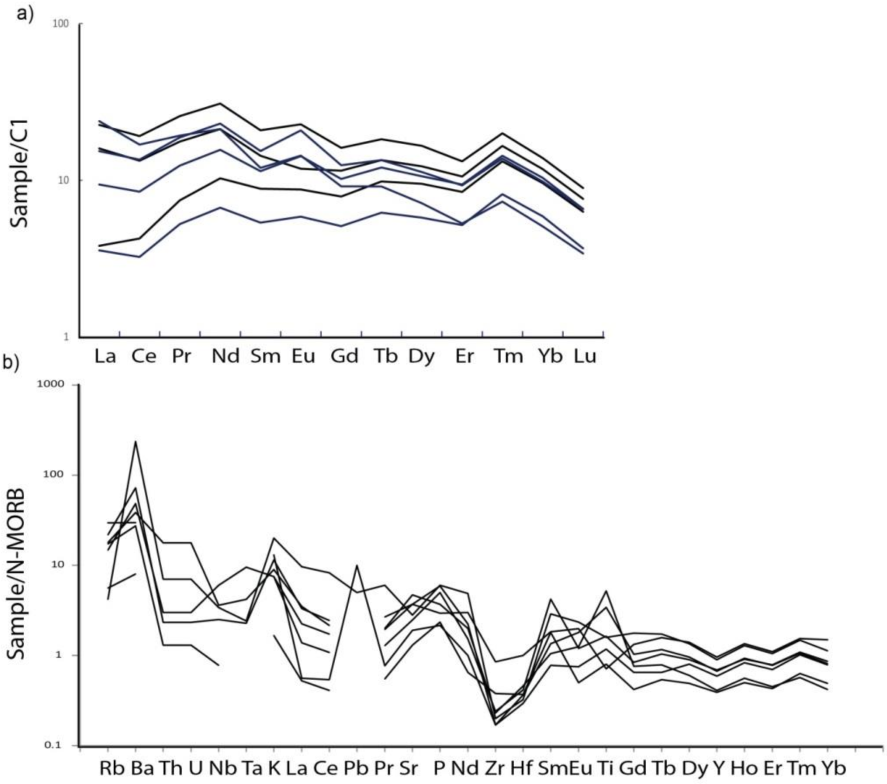

Figure 8. a) Chondrite normalized REE patterns (normalizing values are after 27) and b) N-MORB normalized multi-element diagram (normalizing values are from 28) for the Serow-Torshab gabbros.

Oxygen fugacity and water contents

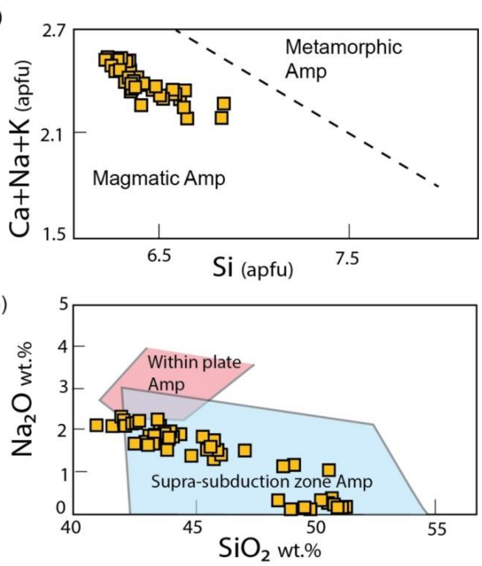

Figure 9. a) Si vs. CNK (apfu) diagram (32), used for distinguishing between magmatic and metamorphic amphiboles, demonstrating the magmatic nature of the examined amphiboles. b) SiO_2 vs. Na_2O diagram in amphiboles (33), indicating that the studied amphiboles belong to the SSZ type.

The elevated presence of amphibole modal percentage in the Serow-Torshab gabbros suggests a notable abundance of H_2O as the primary fluid constituent in the parent magma of the studied rocks. This crucial factor likely influenced the temperature of the liquidus and the composition of the melt. In order to assess the fluid fugacity parameter, mineral chemistry-based diagrams utilizing clinopyroxene and amphibole were employed for analysis (Figure 11a-d). These diagrams, incorporating Al, Na, Ti, Cr, and Mg# values of clinopyroxene, Fe#, and Al content in the amphibole, along with the anorthite content of plagioclases, provide insight into the fluid fugacity of the magma. The fluid content may either originate from inherent source characteristics or be a result of heightened levels due to metasomatic events. Both scenarios are considered relevant in this context. The relatively high anorthite content of plagioclases is typically linked to the crystallization of plagioclase from water-rich magmas, suggesting derivations from a melt with high water content during crystallization (39).

Geothermobarometry

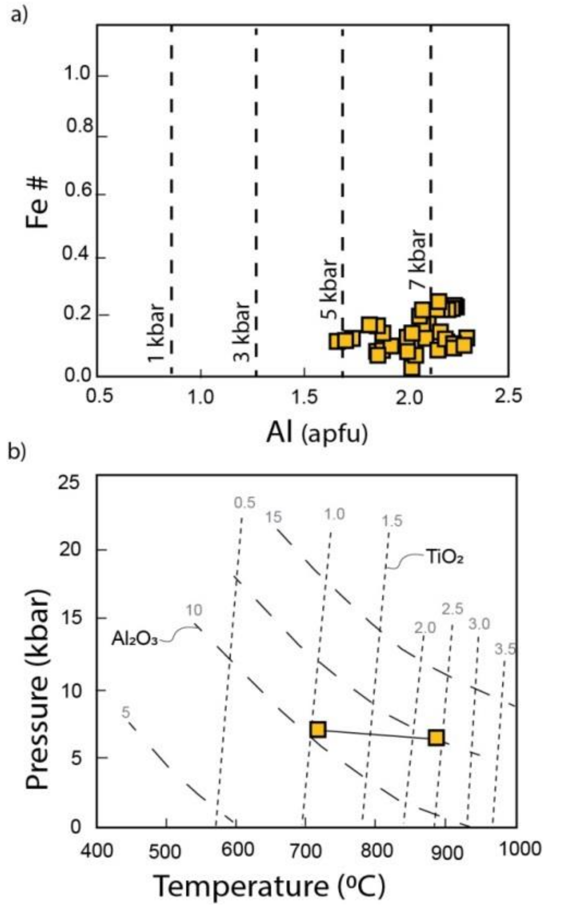

Figure 12. a) Pressure estimation for the Serow-Torshab gabbro utilizing total Al content vs. Fe# in amphiboles (44), indicating a pressure range of 5-8 kbar. b) Pressure-Temperature (PT) grid based on amphibole Al_2O_3 and TiO_2 content (45; max and min values), corroborating the aforementioned pressure range and temperature of 700-900°C.

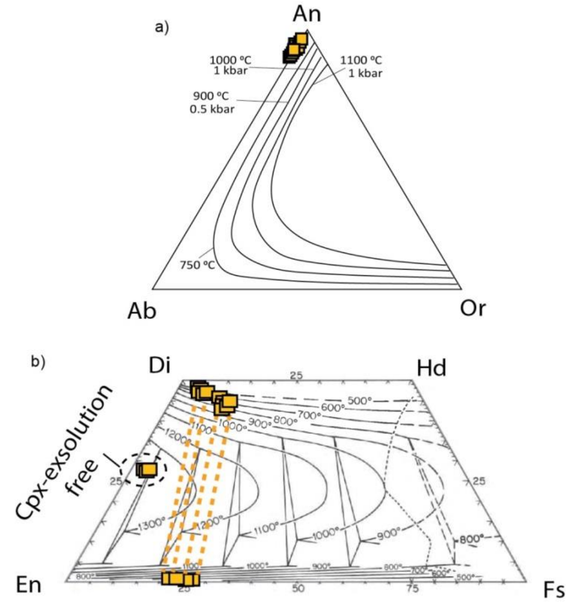

Figure 13. a) Thermometry diagrams for the feldspars (46) suggesting a crystallization temperature of 1000°C for the Serow-Torshab gabbro. b) Solvus thermometry for pyroxene in the Serow-Torshab gabbro (47). Exsolution-free clinopyroxenes crystallized up to 1300°C, whereas clinopyroxenes equilibrated with orthopyroxenes exhibit temperatures of 800-900°C.

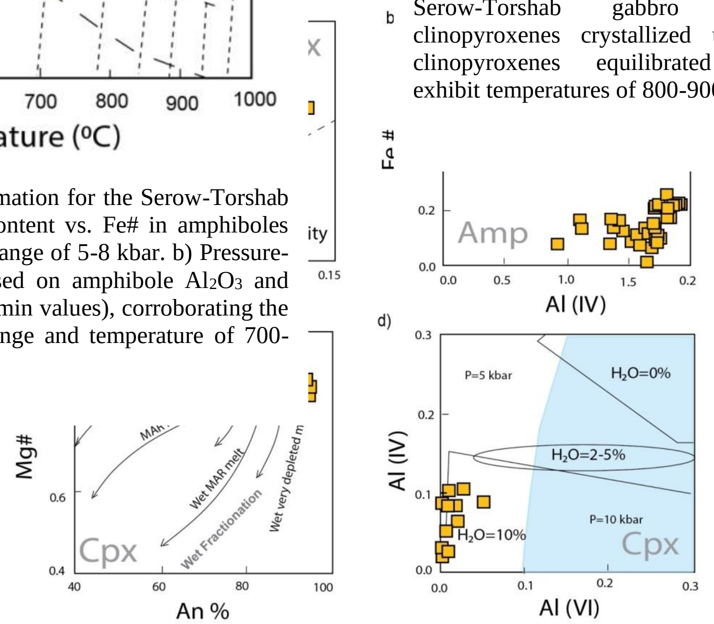

Figure 11. Estimation of oxygen fugacity for the parental magma of the Serow-Torshab gabbro. a) Based on clinopyroxene (40) and b) Based on amphibole (41), both indicating high oxygen fugacity; c) Plagioclase anorthite content vs. Mg# (42) revealing a highly depleted melt with a wet composition for the gabbro magma; d) Al content in clinopyroxene (43) indicating a high water abundance (10%) in the magma, suggesting emplacement in a low-pressure setting (5 kbar).

Amphibole and pyroxene chemistry serve as valuable parameters for assessing crystallization pressure and temperature. Various geothermobarometers were applied to estimate the crystallization conditions of the Serow-Torshab gabbros. The plot of total Al content (apfu) against Fe# in amphiboles represents a crystallization pressure range of 5-8 kbar (Figure 12a, b), corresponding to a temperature range of 700-900°C (Figure 12b).

The feldspar diagram suggests temperatures below 750°C for mineral formation in the Serow-Torshab

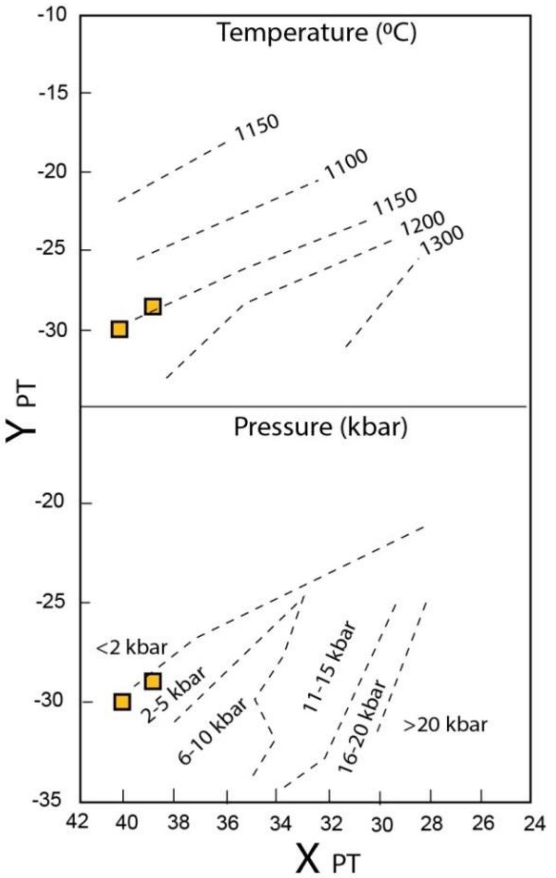

Figure 14. X_{PT} vs. Y_{PT} diagram (by 48), based on clinopyroxene composition (max and min values), suggests a pressure of 2-5 kbar and temperature of 1150 ºC for Serow-Torshab gabbro. The factors are calculated as below:

$$X_{PT}=0.446SiO_2+0.187TiO_2-0.404Al_2O_3+0.346FeO-0.052MnO+0.309MgO+0.431CaO-0.446Na_2O$$

$$Y_{PT}=-0.369SiO_2+0.535TiO_2-0.317Al_2O_3+0.323FeO+0.235MnO-0.516MgO-0.167CaO-0.153Na_2O$$

gabbroic rocks (Figure 13a, following reference 46). Utilizing solvus curve-based pyroxene thermometry (as proposed by 47) indicates temperatures ranging from 800°C to 1000°C (Figure 13b) for the exsolution lamellas of clino-/orthopyroxene, which aligns well with the findings of other thermometers. However, exsolution-free clinopyroxenes exhibit slightly higher temperatures (>1300°C; Figure 13b), implying that the individual clinopyroxenes were crystallized at higher temperatures than the others. However, the exsolution-bearing ones equilibrated at 300-400 ºC lower than the exsolution free ones, during the sub-solidus events. An alternative calibration method (as described in 48) provides temperatures of 1150 °C at pressures of 2-5 kbar for the crystallization of clinopyroxene in the Serow-Torshab gabbros (Figure 14). Such conditions were confirmed for the other ophiolite related mafic (gabbric) intrusions in the Neo-Tethyan suture like, in the Chaldoran, south of Maku (49) or in the west of Maku region (50).

Conclusions

The Serow ophiolite-related gabbro in the Torshab area, situated in northwest Iran near Urmia, is part of the Mesozoic Neo-Tethyan ophiolitic belt.

The examined gabbros exhibit characteristics of arc-related rocks and display signs of metasomatic enrichment, likely originating from oceanic slab-derived melt/fluids.

Mineral chemistry studies on the gabbros offer insights into the geodynamic setting, formation conditions, and magmatic processes, providing valuable information for understanding the tectonic evolution of the region.

The geochemical signatures suggest that the derivation of the Torshab gabbro occurred from a melt with high water content during crystallization.

The formation pressure-temperature conditions, fluid fugacity, and geochemical feature, points to a supra-subduction setting for the Serow-Torshab ophiolitic gabbros. The Serow Late Cretaceous ophiolite was generated within an SSZ situation, exhumed, and emplaced in the Late Cenozoic, throughout collisional events.

Acknowledgments

This work was economically reinforced by Urmia University. The authors would like to thank Dr. Dirk Müller for his significant help in performing EPMAs and Prof. Javad Gholami for English editing. In addition, we appreciate the two anonymous reviewers' constructive comments.

References

1. Modjarrad M, Whitney DL, Omrani H. Petrologic evolution of the Gysian ophiolitic serpentinites, NW Iran. Acta Geochimica. 2024a; https://doi.org/10.1007/s11631-024-00682-6
2. Modjarrad M, Moayyed M. Geochemistry of Central part of the NeoTethys Suture zone serpentinites (From NW Iran to Iraqi Zagros and Eastern Anatoly). Iranian Journal of Geology. 2024b;18 (69):49-66 (in Persian with English abstract).
3. Moghadam HS, Li Q, Griffin W, Stern R, Santos J, Lucci F, Beyarslan M, Ghorbani G, Ravankhah A, Tilhac R. Prolonged magmatism and growth of the Iran-Anatolia Cadomian continental arc segment in Northern Gondwana. Lithos. 2021; 384, 105940.

4. Saccani E, Allahyari K, Beccaluva L, Bianchini G. Geochemistry and petrology of the Kermanshah ophiolites (Iran): implication for the interaction between passive rifting, oceanic accretion, and OIB-type components in the Southern Neo-Tethys Ocean. Gondwana Research. 2013; 24 (1):392–411.
5. Putirka KD. Thermometers and barometers for volcanic systems. Reviews in Mineralogy and Geochemistry. 2008; 69:61- 120.
6. Heliker C. Inclusions in Mount St. Helens dacite erupted from 1980 through 1983. Journal of Volcanology and Geothermal Research. 1995; 66:115–135.
7. Hickey-Vargas R, Abdollahi MJ, Parada MA, Frey FA. Crustal xenoliths from Calbuco volcano, Andean southern volcanic zone: implications for crustal composition and magma-crust interaction. Contributions to Mineralogy and Petrology. 1995; 119:331–344.
8. Beard JS, Borgia A. Temporal variation of mineralogy and petrology in cognate gabbroic enclaves at Arenal volcano, Costa Rica. Contributions to Mineralogy and Petrology. 1989; 103:110–122.
9. Costa F, Dungan MA, Singer BS. Hornblende- and Phlogopitebearing gabbroic xenoliths from Volcan San Pedro (36 S), Chilean Andes: evidence for melt and fluid migration and reactions in subduction-related Plutons. Journal of Petrology. 2002; 43(2):219–241.
10. Modjarrad M. Geochemistry and crystal shape, size and spatial distribution in arc-related gabbro, Urmia, NW Iran. Acta Geochimica. 2022; doi.org/10.1007/s11631-022-00557-8.
11. Moghadam SH, Li QL, Stern RJ, Chiaradia M, Karsli O, Rahimzadeh B. The Paleogene Ophiolite Conundrum of the Iran-Iraq Border Region. Journal of the geological society of America. 2020; doi: https://doi.org/10.1144/jgs2020-009.
12. Haghipour A, Aghanabati A. 1:250000 geological sheet of Serow. Geological survey of Iran. 1973; Tehran.
13. Aghanabati A, Haghipour A. 1:100000 geological sheet of the Gangechin (Serow). Geological survey of Iran. 1990; Tehran.
14. Berberian M, King GCP. Towards a paleogeography and tectonic evolution of Iran. Canadian Journal of Earth Sciences. 1981; 18:210-265.
15. Mazhari SA, Bea F, Amini S, Ghalamghash J, Molina JF, Montero MP, Scarrow J, Williams IS. The Eocene bimodal Piranshahr massif of the SSZ, NW Iran: a marker of the end of the collision in the Zagros orogen. Journal of the Geological Society. 2009; 166:53-69.
16. Asadpour M, Pourmoafi SM, Heuss S. Geochemistry, petrology and U-Pb geochronology of Ghazan mafic-ultramafic intrusion, NW Iran. Petrology. 2013; 4 (14):1-16. (in Persian with English abstract).
17. Rahimsuri Y. Mineralogy and Reserve Evaluation of Khanik-Gazan Titanium Placer Deposit, Urmia, Northwest Iran. New findings in applied geology. 2017; 11(22); 65-79.
18. Whitney DL, Evans BW. Abbreviations for names of rock-forming minerals. American Mineralogist. 2010; 95(1):85-187.
19. Deer WA, RA Howie, Zussman J. An Introduction to the Rock Forming Minerals, Seconded. – Longman Scientific and Technical. 1992; 696 pp.
20. Leake BE, Woolley AR, Arps CES, Birch WD, Gilbert MC, Grice JD, Hawthorne FC, Kato A, Kisch HJ, Krivovichev VG, Linthout K, Laird J, Mandarino JA, Maresch WV, Nickel EH, Rock NMS, Schumacher JC, Smith DC, Stephenson NCN, Ungaretti L, Whittaker EJW, Youshi G. Nomenclature of amphiboles: report of the subcommittee on amphiboles of the International Mineralogical Association, commission on new minerals and mineral names. American Mineralogist. 1997; 82:1019–1037.
21. Pearce JA, Reagan MK. Identification, classification, and interpretation of boninites from Anthropocene to Eoarchean using Si-Mg-Ti systematics. Geosphere. 2019; 15 (4):1008-1037.
22. Pearce JA. Geochemical fingerprinting of oceanic basalts with applications to ophiolite classification and the search for Archean oceanic crust. Lithos. 2008; 100:1–4. https://doi.org/10.1016/j.lithos.2007.06.016
23. Saccaini E. A new method of discriminating different type of post-Archen Ophiolitic basalts and their tectonic significance using Th-Nb and Ce-Dy-Yb systematics. Geosciences Frontiers. 2015; 6:481–501.
24. McDonough WF, Sun SS, Ringwood AE, Jagoutz E, Hofmann AW. Potassium, rubidium, cesium in the Earth and Moon and the evolution of the Earth's mantle. Geochimca et Cosmochimica Acta. 1992; 56:1001–1012.
25. Beard JS. Characteristic mineralogy of arc-related cumulate gabbros: implications for the tectonic setting of gabbroic plutons and for andesite genesis. Geological Society of America. 1986; 14:848–851.
26. Vermeesch P. Tectonic discrimination diagrams revisited. Geochemistry Geophysics Geosystems. 2006; 7:1–55.
27. Taylor SR, McLennan SM. The Continental Crust: Its composition and evolution; an examination of the geochemical record preserved in sedimentary rocks. Blackwell, Oxford. 1985; 312p.
28. Sun SS, McDonough WF. Chemical and isotopic systematics of oceanic basalts: Implications for mantle composition and processes. In Saunders AD, Norry MJ (Eds), (1989; 42:313–345). Magmatism in the Ocean Basins: Geological Society Special Publication. https://doi.org/10.1144/GSL.SP.1989.042.01.19.
29. Perfit MR, Gust DA, Bence AE, Arculus RJ, Taylor SR. Chemical characteristics of island-arc basalts: Implications for mantle sources. Chemical Geology. 1980; 30 (3):227-256. https://doi.org/10.1016/0009-2541(80)90107-2.
30. Aldanmaz E, Pearce JA, Thirlwall MF, Mitchell JG. Petrogenetic evolution of Late Cenozoic, post-collision volcanism in western Anatolia, Turkey. Journal of Volcanology and Geothermal Research. 2000; 102:67–95.
31. Rollinson H. Using geochemical data: evolution, presentation, interpretation. Longman Scientific and Technical Press, Harlow. 1995.
32. Giret A, Bonin B, Leger JM. Amphibole compositional trends in oversaturated and undersaturated alkaline plutonic ring-complexes. Canadian Mineralogist. 1980; 18:481-495.
33. Coltorti M, Bonadiman C, Faccini B, Ntaflos T, Siena F. Slab melt and intraplate metasomatism in Kapfenstein mantle xenoliths (Styria Basin, Austria. In: Coltorti M, Downes H, Piccardo GB (Eds), Melting, Metasomatism and Metamorphic Evolution in the Lithospheric Mantel. Lithos

Special Issue. 2007; 94: 66–89.
34. Beccaluva L, Macciotta GB, Piccardo Zeda O. Clinopyroxene composition of ophiolite basalts as petrogenetic indicator. Chemical Geology. 1989; 77:165-182.
35. Burns LE. The Border Ranges ultramafic and mafic complex, south central Alaska: cumulate fractionates of island arc volcanics. Canadian Journal of Earth Sciences. 1985; 22:1020-1038.
36. Parlak O, Höck V, Delaloye M. The suprasubduction zone Pozantı-Karsantı ophiolite, southern Türkiye: evidence for high-pressure crystal fractionation of the ultramafic cumulates: Lithos. 2002; 65:205-224.
37. Loucks RR. Discrimination of ophiolitic from nonophiolitic ultramafic- mafic allochthons in orogenic belts by the Al/Ti ratio in clinopyroxene. Geology. 1990; 18:346-349.
38. Rezaii L, Moazzen M. Mineral chemistry of the ophiolitic peridotites and gabbros from the Serow area: Implications for tectonic setting and locating the Neotethys suture in NW Iran. Central European Geology. 2014; 57 (4):385–402. DOI: 10.1556/CEuGeol.57.2014.4.
39. Bennett EN, Lissenberg CJ, Cashman KV. The signifcance of plagioclase textures in mid ocean ridge basalt (Gakkel Ridge, Arctic Ocean). Contributions to Mineralogy and Petrology. 2019; 174:49.
40. Schweitzer EL, Papike JJ, Bence E. Statistical analysis of clinopyroxene from deep sea basalts. American Mineralogist. 1979; 64:501- 513.
41. Anderson JL, Smith DR. The effect of temperature and oxygen fugacity on Al- inhornblende barometry. American Mineralogist. 1995; 80:549- 559.
42. Kavassnes AJS, Strand HA, Moen Eikeland H, Pedersen RB. The Lyngen gabbro: the lower crust of Ordovician incipient arc. Contributions to Mineralogy and Petrology. 2004; 148:358- 379.
43. Helz RT. Phase reactions of basalts in their melting range at PH2O=5kb as a function of oxygen fugacity. Journal of Petrology. 1973; 17:139–193.
44. Schmidt MW. Amphibole composition in tonalite as a function of pressure: an experimental calibration of the AI-in- hornblende barometer. Contributions to Mineralogy and Petrology. 1992; 110:304- 310.
45. Ernst WG, Liu J. Experimental phase-equilibrium study of Al- and Ti-contents of calcic amphibole in MORB; a semiquantitative thermobarometer. American Mineralogist. 1998; 83 (9-10):952–969.
46. Seck HA. Koexistierende Alkalifeldspate and Plagioklase in system NaAlSi3O8-KAlSi3O8- CaAl2Si2O8 bei Temperaturen 650˚C bis 900˚C. Neues Jahrbuch fur Mineralogie Abhandlungen, 1971; 115:315- 34.
47. Lindsley DH. Pyroxene geothermometry. American Mineralogist. 1983; 68:477- 493.

48. Soesoo A. A multivariate statistical analysis of clinopyroxene composition: Empirical coordinates for the crystallisation PT-estimations. Geological Society of Sweden (Geologiska Föreningen). 1997; 119:55–6.
49. Moazzen M, Bargoshadi MR, Yang TN. Early Cretaceous (Albian) intra-oceanic subduction in northern branch of Neotethys in NW Iran: U–Pb geochronology and geochemistry of ophiolitic metagabbros from the Chaldoran area. Geological Journal. 2020; 1–20. DOI: 10.1002/gj.4018.
50. Modjarrad M. Mineral chemistry and geochemistry of trace and rare earth elements in the ultramafic rocks of west of Maku. Iranian Geological Journal. in press; (in Persian with English abstract).